Supplementary Information

Exploration and Evaluation of Proton Sources Assisted Photocatalyst for Hydrogen Generation

T. C. Bhagya[a], Athira Krishnan[b], Arunima Rajan S[a], M. Ameen Sha[a], B. R. Sreelekshmy[c], P. Jineesh[a], S. M. A. Shibli[a*,]

***Corresponding author:** S. M. A. Shibli, E-mail: smashibli@yahoo.com, Tel: +91 8547067230.

Number of pages in the supporting information: 12

Number of figures in the supporting information: 12

Number of tables in the supporting information: 2

Content

Fig. S7. Apparent quantum efficiency of photocatalytic hydrogen generation with the 1.5:1 Fe_2O_3-TiO_2, 1:1 Fe_2O_3-TiO_2, 1:1.5 Fe_2O_3-TiO_2 systems under visible light irradiation

Fig. S8. N_2 adsorption and desorption isotherm of (A)1:1 Fe_2O_3-TiO_2, (B) 1:1.5 Fe_2O_3-TiO_2, (C) 1.5:1 Fe_2O_3-TiO_2; and (D) the corresponding surface area, S_{BET} values of, (a) 1:1.5 Fe_2O_3-TiO_2, (b)1:1 Fe_2O_3-TiO_2, (c)1.5:1 Fe_2O_3-TiO_2

Fig. S9. GC analysis of (a) pure hydrogen (standard); (b) hydrogen generated from the proton source assisted Fe_2O_3-TiO_2 photocatalyst under visible light irradiation ($\lambda > 420$ nm)

Fig. S10. X-ray diffraction patterns of the 5 w/v% 1.5:1 Fe_2O_3-TiO_2, before and after photocatalytic test (PCT)

Fig. S11a. Lifetime evaluation of the photogenerated electrons for Fe_2O_3-TiO_2 photocatalyst from Time-resolved fluorescence

Fig. S11b. Nyquist plots of (a) Fe_2O_3, (b) TiO_2, and (c) Fe_2O_3-TiO_2

Table S1. Elemental composition of Fe_2O_3-TiO_2 photocatalyst

Table S2. Comparison of the photocatalytic activity with some reported systems

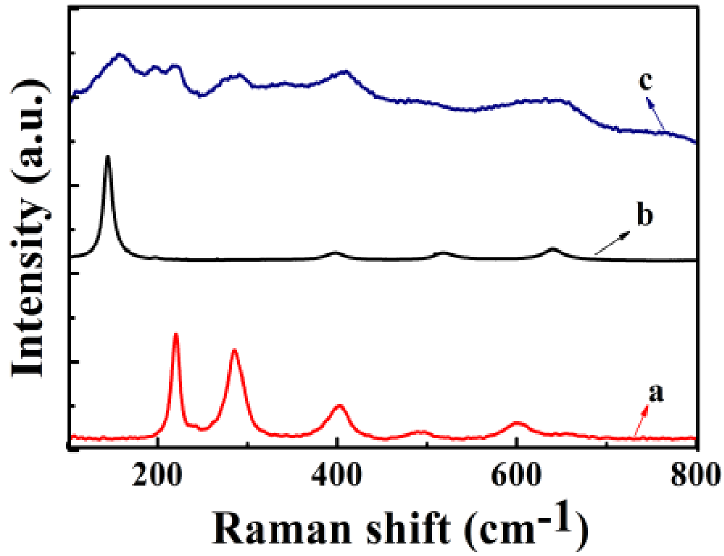

Fig. S1. Raman spectra of (a) pure Fe_2O_3, (b) pure TiO_2, and (c) Fe_2O_3-TiO_2

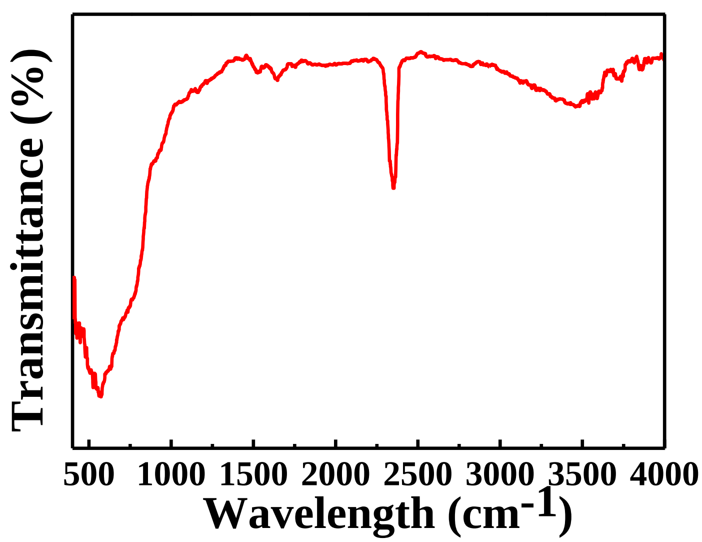

Fig. S2. FT-IR spectra of Fe_2O_3-TiO_2 photocatalyst

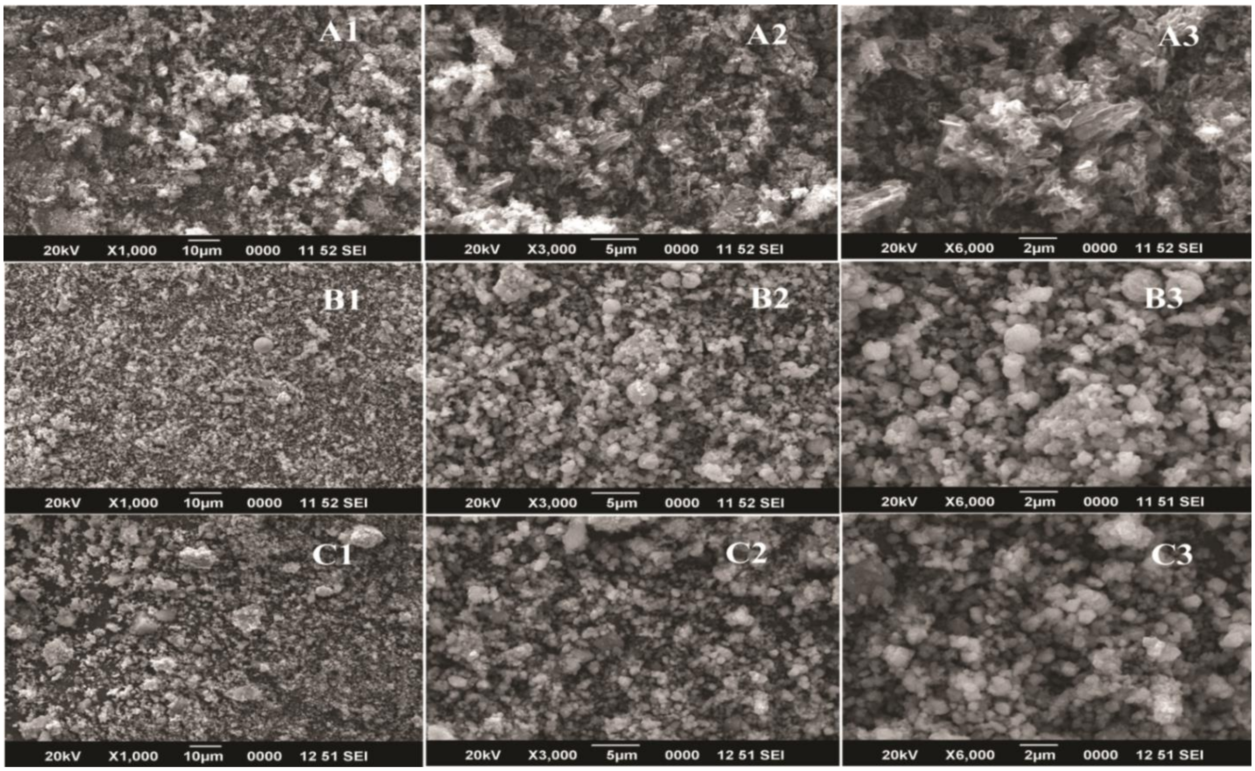

Fig. S3. SEM images of (A1, A2, A3) pure Fe_2O_3, (B1, B2, B3) pure TiO_2, and (C1, C2, C3) Fe_2O_3-TiO_2 (at magnifications 1000 X, 3000 X, 6000 X)

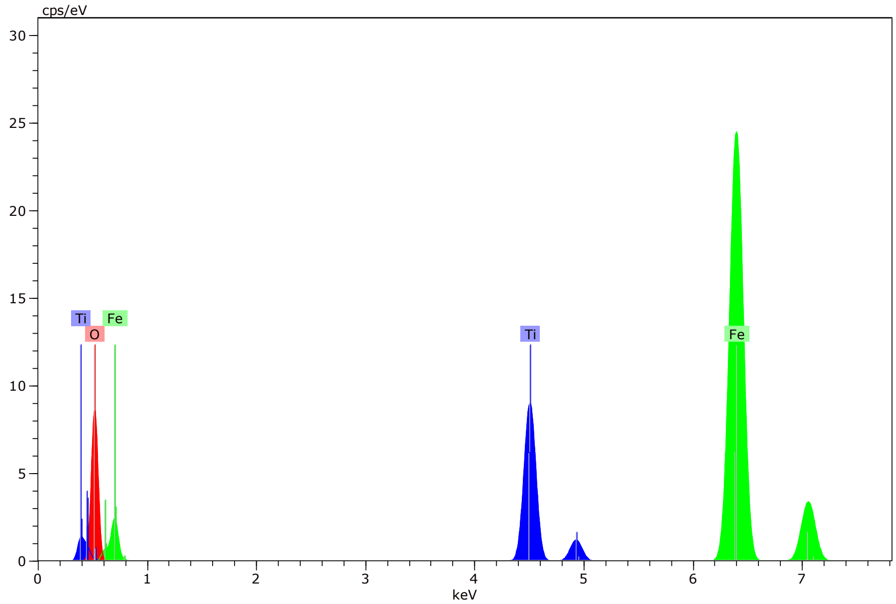

Fig. S4. EDX spectrum of Fe_2O_3-TiO_2 photocatalyst

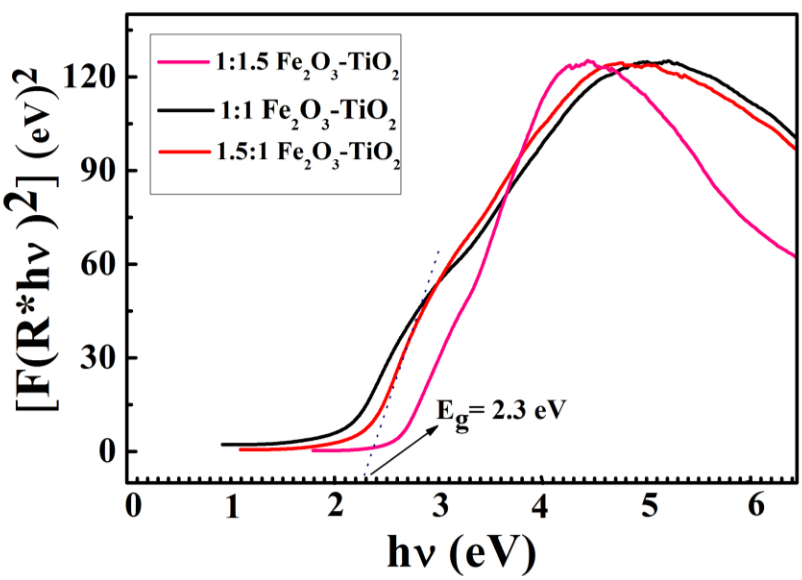

Fig. S5. Plot of transformed Kubelka - Munk function as a function of the energy of light for 1:1.5 Fe_2O_3-TiO_2, 1:1 Fe_2O_3-TiO_2, 1.5:1 Fe_2O_3-TiO_2

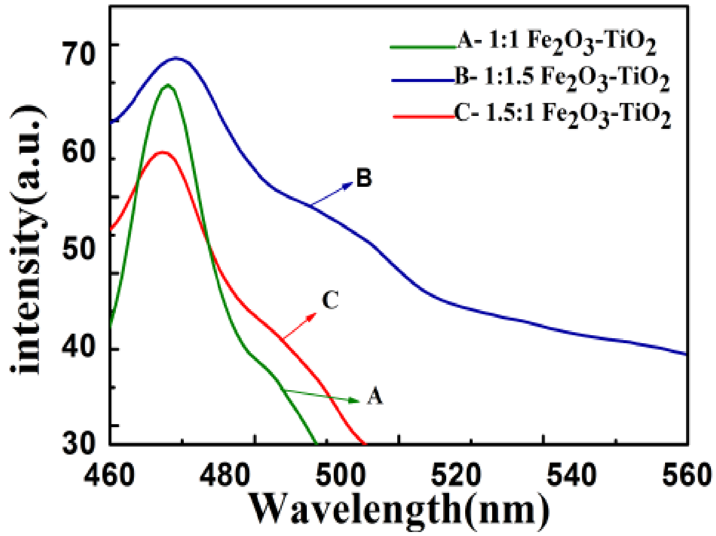

Fig. S6. Photoluminescence (PL) spectra of 1:1 Fe_2O_3-TiO_2 (A); 1:1.5 Fe_2O_3-TiO_2 (B); 1.5:1 Fe_2O_3-TiO_2 (C), using the excitation wavelength of 430 nm

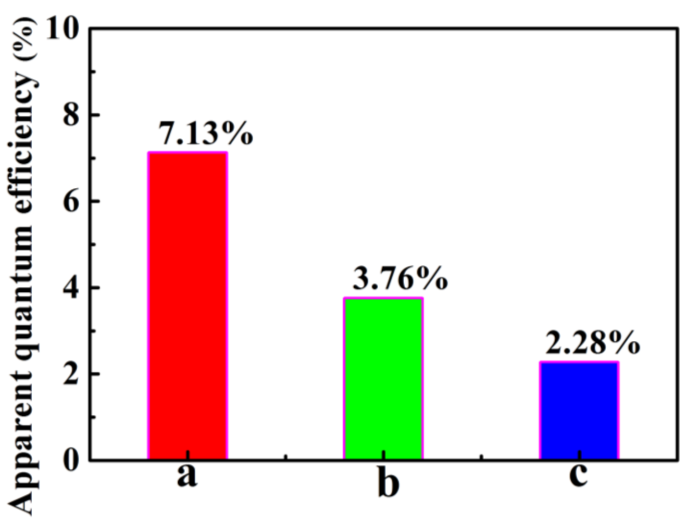

Fig. S7. Apparent quantum efficiency of photocatalytic hydrogen generated with (a) 1.5:1 Fe_2O_3-TiO_2; (b) 1:1 Fe_2O_3-TiO_2; and (c) 1:1.5 Fe_2O_3-TiO_2 systems under visible light irradiation

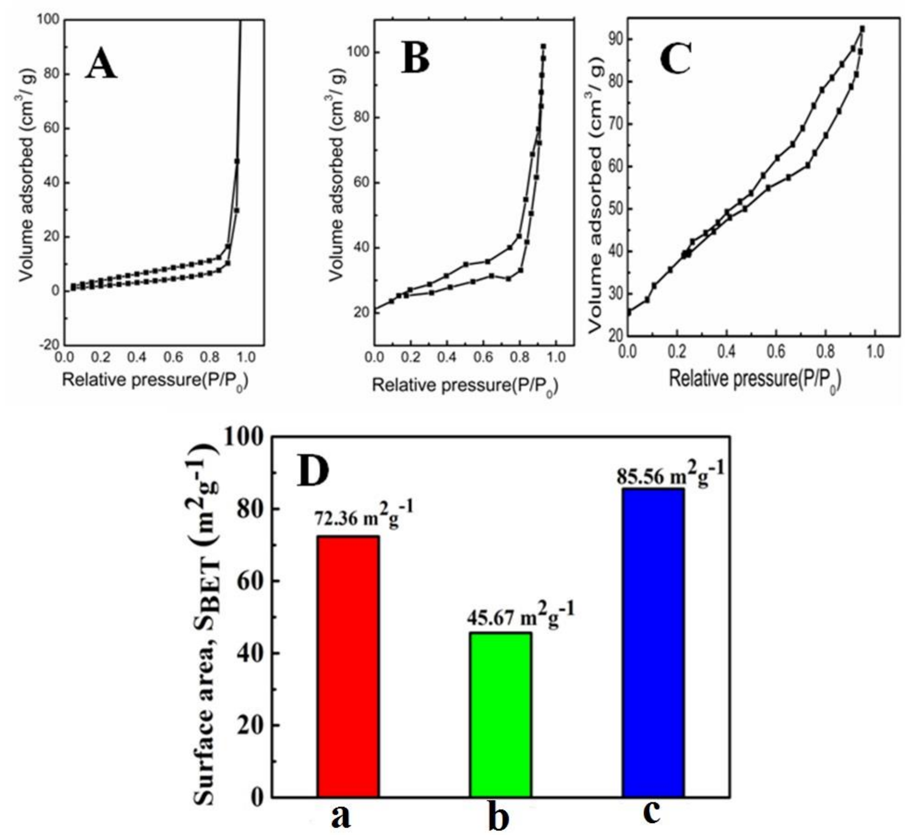

Fig. S8. N_2 adsorption and desorption isotherm of (A)1:1 Fe_2O_3-TiO_2, (B) 1:1.5 Fe_2O_3-TiO_2, (C) 1.5:1 Fe_2O_3-TiO_2; and (D) the corresponding surface area, S_{BET} values of, (a) 1:1.5 Fe_2O_3-TiO_2, (b)1:1 Fe_2O_3-TiO_2, (c)1.5:1 Fe_2O_3-TiO_2

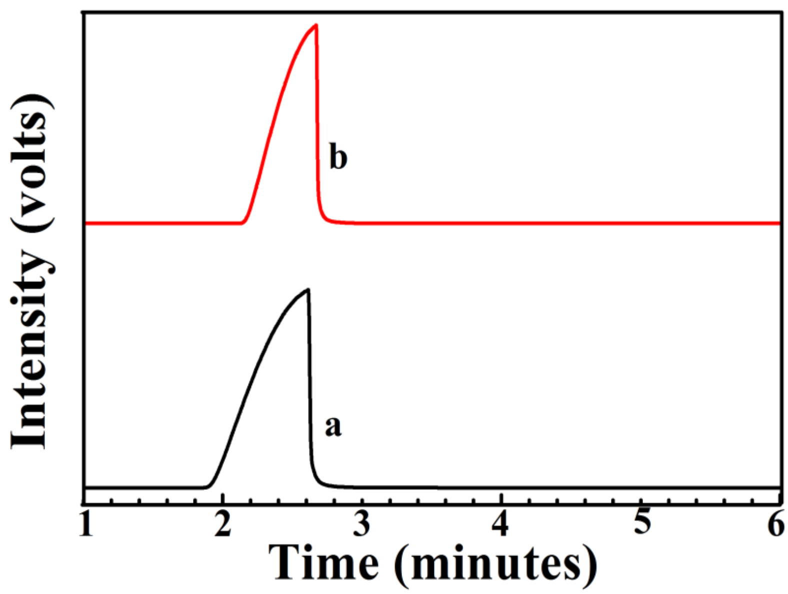

Fig. S9. GC analysis of (a) pure hydrogen (standard); (b) hydrogen generated from the proton source assisted Fe_2O_3-TiO_2 photocatalyst under visible light irradiation (λ > 420 nm)

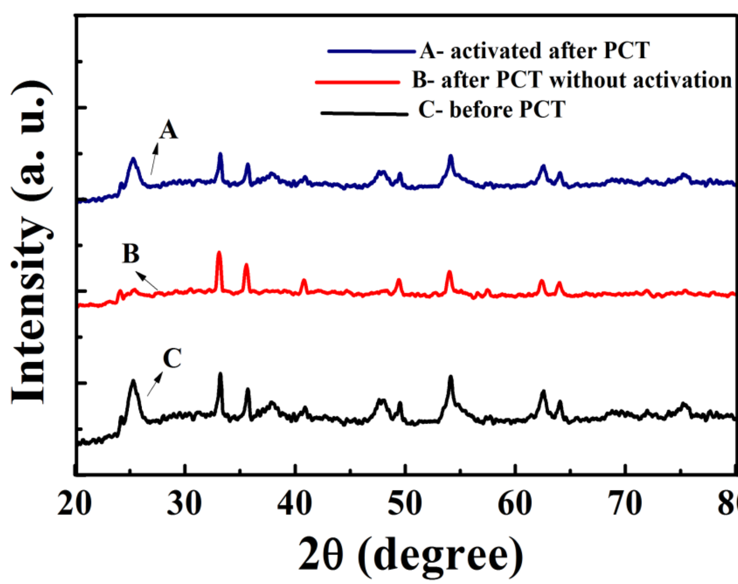

Fig. S10. X-ray diffraction patterns of the 5 w/v% 1.5:1 Fe_2O_3-TiO_2, before and after photocatalytic test (PCT)

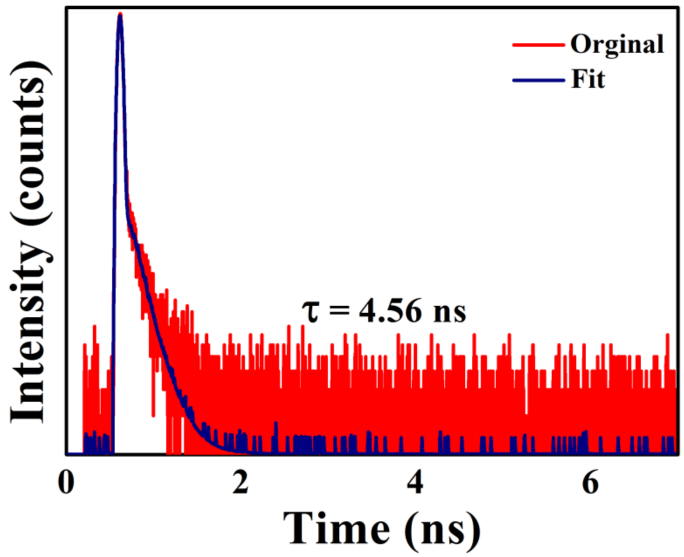

Fig. S11a. Lifetime evaluation of the photogenerated electrons for Fe_2O_3-TiO_2 photocatalyst from Time-resolved fluorescence

$$Y = \sum Ai\ e^{t/\tau_i} \quad (i = 1, 2) \qquad (1)$$

$$\tau = (A_i \tau_i^2) / (A_i \tau_i)\ (i = 1, 2) \qquad (2)$$

Bi-exponential decay kinetics as in equation 1 is used to get the best fit of the Time-resolved fluorescence data, and the average lifetime is calculated using equation 2

Where t, τ_i and A_i are constants, the value of which are obtained by fitting the decay curves.

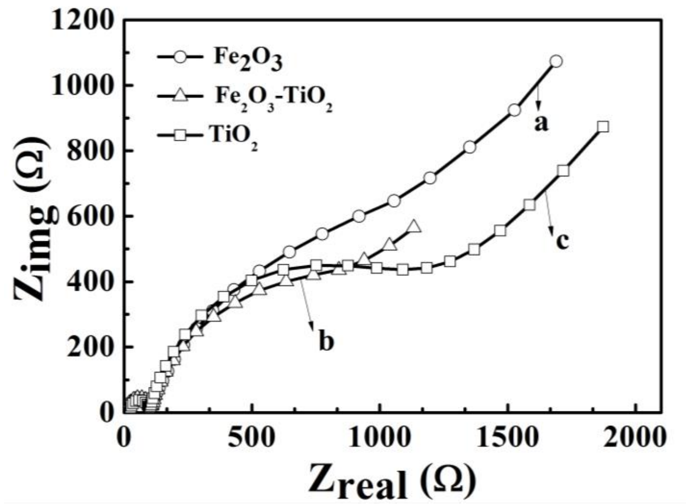

Fig. S11b. Nyquist plots of (a) Fe_2O_3, (b) TiO_2, and (c) Fe_2O_3-TiO_2

Table S1. Elemental composition of Fe_2O_3-TiO_2 photocatalyst

Element	**Weight%/STEM-EDX**	**Weight%/ICP-MS**
Ti	26.16	28.475
Fe	50.34	53.74
O	23.50	

Table S2. Comparison of the photocatalytic activity with some reported systems.

Parameter	[R1][67]	[R2][68]	[R3][69]	[R4][70]	[R5][71]	[R6][72]	[R7][73]	[R8][74]	[R9][75]	[R10][76]	[R11][77]	[R12][78]	[R13][79]	Present work
Catalytic system	TiO_2-ZrO_2 hollow spheres	Pt-CeO_2	Pt/TiO_2	Pt/Colloidal WO_x wires	Fe_3O_4@SnO_2@MoS_2/g-C_3N_4 spheres	Cu_2ZnSnS_4/Ag/PANI	Fe_2O_3-TiO_2 hierarchical structure	CuS-TiO_2/Pt	MoS_2/B-TiO_2 sheets	Fe_2O_3/g-C_3N_4	α-Fe_2O_3	CoP-CdS	TiO_2/NiS	Fe_2O_3-TiO_2
%Composition	-	1 wt% Pt-CeO_2	0.17% Pt/TiO_2	1 wt% Pt loaded WO_x	2.0 atm % of MoS_2/g-C_3N_4	30 mg CZTS	H-Fe_2O_3/TiO_2 -2%	1.97 atomic% Pt, CuS-TiO_2 (1:2)	1.0 wt% MoS_2 + B-TiO_2	FCN containing 0.02 wt% Fe	α, γ-Fe_2O_3 (500 °C)	1 wt%-CoP-CdS	3.3 mol% NiS	1.5:1 Fe:Ti (5% w/v)
Particle size	-	< 10 nm	-	< 3 nm	~0.481 μm	< 40 nm	~ 33 nm	Average diameter (40-60 nm)	Length 1 μm, width 1 μm, thickness 0.4 μm	<20 nm	~27 nm	-	diameter- 300 nm, length 10 μm	10 nm
Surface area	53.6 m^2g^{-1}	119.4 m^2g^{-1}	54 m^2g^{-1}	-	46.71 m^2g^{-1}	-	28 cm^2 g^{-1}	15.87 m^2g^{-1}	35.6 m^2g^{-1}	63.4 m^2g^{-1}	57 m^2g^{-1}	7.23 m^2g^{-1}	30 m^2g^{-1}	85.56 m^2g^{-1}
Sacrificial agents/ electron donors	Na_2S	ethanol	formaldehyde	Methanol	Triethanolamine	Na_2S, Na_2SO_3	Na_2S/Na_2SO_3	Na_2S/Na_2SO_3	Methanol	Triethanolamine	Na_2SO_3	Na_2S/Na_2SO_3	methanol	Diethyl amine hydrogenchloride (as proton source)
Hydrogen production rate	23.7 μmol/8 h	93.43 μmol/2h	2.28 μmol min^{-1}	464 μmol h^{-1}	110.72 μmol h^{-1}	859.6 μmol h^{-1}	217.6 μmol h^{-1}	746 μmol h^{-1}	0.50 mmol h^{-1}	77.6 μmol h^{-1}	<5 mL	< 60 mmol g^{-1}	655 μmol h^{-1}	880 μmol h^{-1}
Quantum efficiency	-	1.57%	10.91%	-	-	30.5%	0.94%	1.55%	-	-	0.26%	11.6%	-	19.39%
Cyclic stability	≤ 91.4% for 3 cycles	1.52 mmol (34 h)	Reliable stability (4 cycles of 3h each)	Not mentioned	Retained stability (5 cycles of 4 h each)	Retained stability (4 cycles of 5 h each)	~1500 μmol /7 h	Retained stability (5 cycles of 2 h each)	Retained (5 cycles of 5 h each)	Retained stability (5 cycles of 6 h each); <500 μmol/6 h	-	< 55 mmol g^{-1} (for 5 cycles of 4 h each)	Retained stability (4 cycles of 3 h each)	Retained stability (4 cycles of 6 h each); >2500 μmol/6 h

References

67 J. Zhang, L. Li, Z. Xiao, D. Liu, S. Wang, J. Zhang, W. Zhang, Hollow sphere TiO_2–ZrO_2 prepared by self-assembly with polystyrene colloidal template for both photocatalytic degradation and H_2 evolution from water splitting, ACS Sustainable Chem. Eng., 2016, **4**, 2037-2046.

68 N. R Manwar, A. A. Chilkalwar, K. K. Nanda, Y. S. Chaudhary, J. Subrt, S. S. Rayalu, N. K. Labhsetwar, Ceria supported Pt/PtO-Nanostructures: efficient photocatalyst for sacrificial donor assisted hydrogen generation under visible-NIR light irradiation, ACS Sustainable Chem. Eng., 2016, **4**, 2323-2332.

69 P. Chowdhury, G. Malekshoar, M. B. Ray, J. Zhu, A. K. Ray, Sacrificial hydrogen generation from formaldehyde with Pt/TiO_2 photocatalyst in solar radiation, Ind.Eng.Chem. res., 2013, **52**, 5023-5029.

70 T. Paik, M. Cargnello, T. R. Gordon, S. Zhang, H. Yun, J. D. Lee, C. B. Murray, Photocatalytic Hydrogen Evolution from Substoichiometric Colloidal WO_3–x Nanowires, ACS Energy Lett., 2018, **3(8)**, 1904-1910.

71 D. Lu, H. Fan, K. K. Kondamareddy, H. Yu, A. Wang, H. Hao, J. Shen, Highly Efficient Visible-Light-Induced Photocatalytic Production of Hydrogen for Magnetically Retrievable Fe_3O_4@ SiO_2@ MoS_2/g-C_3N_4 Hierarchical Microspheres, ACS Sustainable Chem. Eng., 2018, **6(8),** 9903-9911.

72 X. Wang, Y. Ruan, S. Feng, S. Chen, K. Su, Ag Clusters Anchored Conducting Polyaniline As Highly Efficient Cocatalyst for Cu_2ZnSnS_4Nanocrystals toward Enhanced Photocatalytic Hydrogen Generation, ACS Sustainable Chem. Eng., 2018, **6(9)**, 11424-11432.

73 Zhu, S, F Yao, C. Yin, Y. Li, W. Peng, J. Ma, D. Zhang, Fe_2O_3/TiO_2 photocatalyst of hierarchical structure for H_2 production from water under visible light irradiation, Microporous and Mesoporous Mater., 2014, **190**, 10-16

74 K. Manjunath, V. S. Souza, G. Nagaraju, J. M. L. Santos, J. Dupont, T. Ramakrishnappa, Superior activity of the CuS–TiO_2/Pt hybrid nanostructure towards visible light induced hydrogen production, New J. Chem., 2016, **40(12),** 10172-10180.

75 X. Yang, H. Huang, B. Jin, J. Luo, X. Zhou, Facile synthesis of MoS_2/B-TiO_2 nanosheets with exposed {001} facets and enhanced visible-light-driven photocatalytic H_2 production activity, RSC Adv., 2016, **6(108)**, 107075-107080.

76 Y. P. Li, F. T. Li, X. J. Wang, J. Zhao, J. N. Wei, Y. J. Hao, Y. Liu., Z-scheme electronic transfer of quantum-sized α-Fe_2O_3 modified g-C_3N_4 hybrids for enhanced photocatalytic hydrogen production, Int. J. Hydrogen Energy, 2017, **42(47)**, 28327-28336.

77 S. Boumaza, H. Kabir, I. Gharbi, A. Belhadi, M. Trari, Preparation and photocatalytic H_2-production on α-Fe_2O_3 prepared by sol-gel, Int. J. Hydrogen Energy, 43, 2018, 3424-3430.

78 J. Wang, P. Wang, C. Wang, Y. Ao, In-situ synthesis of well dispersed CoP nanoparticles modified CdS nanorods composite with boosted performance for photocatalytic hydrogen evolution, Int. J. Hydrogen Energy, 2018, **43(32)**, 14934-14943.

79 F. Xu, L. Zhang, B. Cheng, J. Yu, Direct Z-Scheme TiO_2/NiS Core–Shell Hybrid Nanofibers with Enhanced Photocatalytic H_2-Production Activity, ACS Sustainable Chem. Eng., 2018, **6(9)**, 12291-12298.

.